Hindawi Publishing Corporation
Journal of Nanomaterials
Volume 2016, Article ID 3542359, 15 pages
http://dx.doi.org/10.1155/2016/3542359

Research Article

Adsorptive Removal of Acid Blue 80 Dye from Aqueous Solutions by Cu-TiO_2

Ingrid Johanna Puentes-Cárdenas,[1] Griselda Ma. Chávez-Camarillo,[1] César Mateo Flores-Ortiz,[2] María del Carmen Cristiani-Urbina,[3] Alma Rosa Netzahuatl-Muñoz,[4] Juan Carlos Salcedo-Reyes,[5] Aura Marina Pedroza-Rodríguez,[5] and Eliseo Cristiani-Urbina[1]

[1]*Escuela Nacional de Ciencias Biológicas, Instituto Politécnico Nacional, Prolongación de Carpio y Plan de Ayala s/n, Colonia Santo Tomás, 11340 México, DF, Mexico*
[2]*Facultad de Estudios Superiores Iztacala, Universidad Nacional Autónoma de México, Avenida de los Barrios 1, Los Reyes Iztacala, 54090 Tlalnepantla, MEX, Mexico*
[3]*Universidad Autónoma de Chiapas, Boulevard Belisario Domínguez, Kilómetro 1081, s/n, 29000 Tuxtla Gutiérrez, CHIS, Mexico*
[4]*Universidad Politécnica de Tlaxcala, Avenida Universidad Politécnica No. 1, San Pedro Xalcaltzinco, 90180 Tepeyanco, TLAX, Mexico*
[5]*Facultad de Ciencias, Pontificia Universidad Javeriana, Carrera 7 No. 40-62, Bogotá D.C. 11001000, Colombia*

Correspondence should be addressed to Eliseo Cristiani-Urbina; ecristianiu@yahoo.com.mx

Received 21 September 2015; Accepted 8 December 2015

Academic Editor: Pantaleo D. Cozzoli

The adsorption performance of a Cu-TiO_2 composite for removing acid blue 80 (AB80) dye from aqueous solutions was investigated in terms of kinetics, equilibrium, and thermodynamics. The effect of operating variables, such as solution pH, initial dye concentration, contact time, and temperature, on AB80 adsorption was studied in batch experiments. AB80 adsorption increased with increasing contact time, initial dye concentration, and temperature and with decreasing solution pH. Modeling of adsorption kinetics showed good agreement of experimental data with the pseudo-second-order kinetics model. The experimental equilibrium data for AB80 adsorption were evaluated for compliance with different two-parameter, three-parameter, and four-parameter isotherm models. The Langmuir isotherm model best described the AB80 adsorption equilibrium data. The thermodynamic data revealed that the AB80 adsorption process was endothermic and nonspontaneous. Kinetics, equilibrium, and thermodynamic results indicate that Cu-TiO_2 adsorbs AB80 by a chemical sorption reaction.

1. Introduction

Synthetic dyes are extensively used in many industries, such as textiles, printing, paper, leather, rubber, food, cosmetics, plastics, pharmaceuticals, and photography [1].

Large quantities of industrial wastewater containing synthetic dyes are directly discharged into water bodies without treatment, which has caused serious pollution problems in many areas [2] and has been a cause of concern because of the potential health hazards of dyes [3]. Dye-colored wastewater also affects aesthetics and water transparency, as well as the natural equilibrium of aquatic systems resulting from reduced oxygenation of the water bodies, and low photosynthetic activity and viability of aquatic plants due to water coloration [4]. Therefore, the removal of synthetic dyes from contaminated water and wastewater is presently recognized to be essential to protecting aquatic and terrestrial environments and public health and well-being [3].

However, dye-polluted wastewater is among the most difficult industrial wastewater types to treat [5] because most of the synthetic dyes are recalcitrant organic molecules that are highly resistant to microbial degradation, extremely soluble in water, and resistant to heat, light, and oxidizing agents [3, 6].

Among several treatment technologies available for dye removal from aqueous solutions, photocatalytic degradation processes have been found to be efficient technologies for the removal of organic dyes from wastewater [7–10]. In this context, titanium dioxide (TiO_2) has become one of the most promising photocatalysts for complete mineralization of many toxic and nonbiodegradable organic compounds due to its chemical-biological inertness, availability, durability, high photocatalytic activity, long-term stability against photochemical corrosion, high refractive index, excellent optical transmittance, ecofriendly nature, and cost effectiveness [11, 12]. However, to improve the photocatalytic activity of TiO_2 and to extend its photoresponse capacity to the visible region, TiO_2 has been doped with various transition metal ions [12, 13]. A promising TiO_2 dopant is divalent copper [Cu(II)], a relatively abundant metal with low cost that may extend the light absorption to the visible region, modify the TiO_2 valence band spectrum, and improve photocatalytic activity [14, 15].

A crucial and primary stage in photocatalytic processes is the adsorption of reacting substances onto the surface of the photocatalysts [16, 17]. It is well known that photodegradation of organic molecules is closely related to their adsorption on the photocatalyst surface, thus facilitating electron injection from the adsorbed excited molecules to the photocatalyst [11, 18]. Therefore, prior adsorption of organic substances onto the photocatalysts' surface is indispensable for achieving higher photodegradation efficiencies and rates in heterogeneous photocatalysis [11, 14, 18, 19]. Similarly, understanding the effect of environmental parameters (e.g., contact time, solution pH, initial adsorbate concentration, and temperature) on adsorption, as well as the mechanism of adsorption, is essential for understanding the performance of photocatalysts and the kinetics of the photocatalytic reaction and for developing optimized photocatalytic processes [20]. In this context, the mechanism of adsorption can be elucidated from adsorption kinetics, isotherm, and thermodynamic studies.

Hence, the present study assesses the adsorption capacity of a new Cu-TiO_2 photocatalyst for acid blue 80 (AB80) dye, which is an anionic anthraquinone dye widely used in detergents, textiles (e.g., wool and nylon), disinfectants, sterilants, sanitation, cosmetics, pesticides, and preservative applications. AB80 is highly resistant to degradation due to its fused aromatic structure [5, 21] and has been identified by the Canadian Ministers of the Environment and Health as a priority substance because of its potential environmental persistence, bioaccumulation, and toxicity to aquatic organisms [21].

In the present work, a Cu-TiO_2 composite was synthesized and characterized by X-ray diffraction (XRD), field emission scanning electron microscopy (FE-SEM), energy dispersive X-ray spectroscopy (EDS), and UV-Vis scanning spectroscopy, as well as in terms of specific surface area and pore size distribution. Likewise, the effects of important parameters on AB80 adsorption by the Cu-TiO_2 composite, such as solution pH, initial AB80 concentration, contact time, and temperature, were investigated. Besides this, the adsorption mechanism of AB80 onto Cu-TiO_2 was assessed in terms of kinetics, equilibrium, and thermodynamics.

2. Materials and Methods

2.1. Reagents. Acid blue 80 dye (benzenesulfonic acid, 3,3′-[(9,10-dihydro-9,10-dioxo-1,4-anthracenediyl) diimino]bis[2,4,6-trimethyl-, disodium salt]) was obtained from Sigma-Aldrich, USA. Stock acid blue 80 (AB80) dye solution was prepared by dissolving 1 g of the dye in 1 L of distilled deionized water. Test AB80 solutions were prepared by diluting the stock dye solution. The titanium dioxide (TiO_2) USP used in this work is commercialized as a food and pharmaceutical additive and was obtained from Químicos De La 13 Ltd., Bogota, Colombia. Analytical grade $CuSO_4{\cdot}5H_2O$ was obtained from J. T. Baker.

2.2. Preparation and Characterization of the Cu-TiO_2 Composite. The Cu-TiO_2 composite samples were prepared as follows: A 10 g L^{-1} TiO_2 suspension in water and a 1.25 g L^{-1} $CuSO_4{\cdot}5H_2O$ solution in ethanol were separately sonicated for 1 h each; subsequently, the samples were mixed and sonicated for 15 min. The pH of the resulting suspension was adjusted to 9.0 with 1 M NaOH. Afterwards, the solid was separated by centrifugation, washed with distilled deionized water, oven-dried at 40°C for 12 h, and calcined in air at 450°C for 1 h.

The resulting Cu-TiO_2 composite was then characterized in terms of specific surface area, pore volume, and average pore diameter using nitrogen adsorption-desorption at 77.35 K, which was conducted using a gas sorption analyzer (Quantachrome, NOVA 4200e series, USA). The specific surface area was determined from isotherms using the Brunauer-Emmett-Teller (BET) equation, and the pore size distribution was determined using the Barrett-Joyner-Halenda (BJH) method.

The morphological and surface characteristics of Cu-TiO_2 composite were observed using a field emission scanning electron microscope (FE-SEM, JEOL, JSM-7401F) operating at 20 kV, equipped with an energy dispersive X-ray spectrometry (EDS) system. The chemical analysis of Cu-TiO_2 composite was determined by EDS.

Analysis of the crystalline phase of Cu-TiO_2 composite was performed by X-ray diffraction (XRD) using PANalytical X'Pert PRO MOD diffractometer, operated with Cu Kα radiation (wavelength = 1.54050 Å) at 45 kV and 40 mA. XRD patterns were collected in 2θ range from 10 to 90° with a scan rate of 0.026° per 40 s and a step size of 0.026°.

The optical properties of the Cu-TiO_2 composite were studied using UV-Vis spectroscopy in the wavelength range of 240–800 nm. The optical band gap (E_g) was estimated following the procedures described by Mathews et al. [22] and Pihosh et al. [23].

2.3. Determination of the Point of Zero Charge (PZC). The pH at which the adsorbent surface has a neutral net charge is referred to as the point of zero charge (PZC). In the present work, PZC was determined by a batch equilibrium method, following the procedures outlined by Hasan et al. [24].

2.4. Kinetics Studies of AB80 Adsorption and Analytical Methods. Batch kinetics adsorption experiments were conducted

to assess the influence of solution pH, initial AB80 concentration, shaking contact time, and temperature on AB80 adsorption from aqueous solutions by the Cu-TiO_2 composite. All of the experiments were performed in 500 mL Erlenmeyer flasks containing 120 mL of AB80 solution of known concentration and 1 g (dry weight) L^{-1} of Cu-TiO_2. Throughout the course of the experiments, the pH of each AB80 solution was maintained at a constant value (±0.1 units) by periodic checking and adjustment where necessary with 0.1 M HCl or NaOH solutions. Flasks were agitated in a shaker at a constant 120 rpm shaking speed. All AB80 adsorption experiments were performed in the dark to avoid dye removal by photocatalytic processes.

The effect of solution pH levels on Cu-TiO_2 AB80 adsorption was assessed in AB80 solution at 30 mg L^{-1} initial dye concentration with different pH values ranging from 1.0 to 8.0 ± 0.1, at 25 ± 1°C. To examine the influence of initial AB80 concentration on kinetics performance, experiments were conducted with AB80 concentrations ranging from 10 to 150 mg L^{-1}, at 25 ± 1°C. The effect of temperature on the kinetics of AB80 adsorption was studied by varying temperature from 25 to 60 ± 1°C, and two initial AB80 concentrations were used (30 and 120 mg L^{-1}).

To check for AB80 adsorption onto glass, AB80 precipitation, and/or AB80 photolysis, Cu-TiO_2-free controls were run concurrently and under exactly the same operating conditions as those used for the AB80 adsorption experiments. Throughout the experiments conducted in this work, no change in AB80 concentration was detected in the Cu-TiO_2-free controls, which indicates that the observed AB80 removal in the experiments with the Cu-TiO_2 composite was only due to the adsorbent.

Samples were collected after different times of contact between the Cu-TiO_2 composite and AB80 solutions and centrifuged at 8000 rpm for 20 min. The supernatants were subsequently analyzed spectrophotometrically (Genesys 10 UV-Visible, Thermo Electron Scientific Instruments Corporation) at 626 nm wavelength to quantify the residual AB80 concentration.

2.5. Equilibrium Studies of AB80 Adsorption. For the equilibrium adsorption experiments, 1 g L^{-1} of Cu-TiO_2 composite was brought into contact with solutions of different initial AB80 concentrations (10–150 mg L^{-1}) at 25°C, with constant agitation at 120 rpm for 2 h to ensure adsorption equilibrium was reached. Afterward, samples were collected and centrifuged at 8000 rpm for 20 min, and the obtained supernatants were subsequently analyzed for AB80 concentration.

2.6. Estimation of AB80 Adsorption Capacity. The capacity of AB80 adsorption (q_t, mg g^{-1}), which represents the amount of AB80 removed at time t by the unit mass (dry weight) of Cu-TiO_2 composite, was calculated according to the following mass balance relationship:

$$q_t = \frac{(C_0 - C_t)\,V}{W}, \tag{1}$$

where C_0 and C_t (mg L^{-1}) are the initial and residual AB80 concentrations at times $t_0 = 0$ h and $t = t$ (h), respectively, V is the solution volume (L), and W is the dry weight of Cu-TiO_2 composite (g).

2.7. Adsorption Kinetics Modeling. The dynamics of AB80 adsorption onto the Cu-TiO_2 composite were analyzed using the Elovich, fractional power, pseudo-first-order, and pseudo-second-order kinetics models (Table 1), which have been widely used to analyze and understand the adsorption kinetics of dyes by different adsorbents.

2.8. Adsorption Isotherm Modeling. To quantify the relationship between the amount of AB80 adsorbed at equilibrium onto the Cu-TiO_2 composite and the equilibrium solution concentration of AB80, two-parameter (Langmuir, Freundlich, Dubinin-Radushkevich, and Halsey), three-parameter (Sips, Redlich-Peterson, Koble-Corrigan, Toth, and Khan), and four-parameter (Fritz-Schluender) isotherm models (Table 1) were investigated based on the batch equilibrium experimental results.

2.9. Thermodynamic Study. Thermodynamic parameters such as Arrhenius activation energy (E_A) and the changes in activation enthalpy (ΔH^*), entropy (ΔS^*), and Gibbs free energy (ΔG^*) were calculated to describe the thermodynamic behavior of AB80 adsorption onto Cu-TiO_2 (Table 1).

2.10. Statistical and Data Analysis. Three independent replicates confirmed that the AB80 adsorption experiments were reproducible within a 5% error, and mean values are reported herein. AB80 adsorption data were statistically analyzed by analysis of variance (ANOVA; Tukey's method; overall confidence level = 0.05) using GraphPad Prism software version 6.0c (GraphPad Software, Inc.).

All kinetics, isotherm, and thermodynamic parameters of the models were evaluated by nonlinear regression analysis of the experimental data using the MATLAB R2010b software (The MathWorks Inc.). The determination coefficients (r^2), the residual or sum of squares error (SSE), and the root mean squared error or standard error (RMSE) of the estimate, as well as the 95% confidence intervals of the model parameters, were used with the purpose of measuring the goodness-of-fit of the mathematical models. Good curve fitting was indicated by r^2 values close to 1.0, small RMSE and SSE values, and narrow 95% confidence intervals.

3. Results and Discussion

3.1. Characterization of the Cu-TiO_2 Composite. The specific surface area and porosity are important characteristics of adsorbents. Surface area and pore size distribution were analyzed by N_2 adsorption and desorption studies. The adsorption-desorption isotherm and the derived pore size distributions are illustrated in Figure 1. The N_2 isotherm of Cu-TiO_2 is a type IV IUPAC isotherm, which is observed in mesoporous solids. This isotherm also exhibited a type H3 hysteresis loop (Figure 1(a)), which is characteristic of slit-shaped pores [31]. The specific surface area was found to be

Table 1: Kinetic, isotherm, and thermodynamic models.

Kinetics models			
Elovich	$q_t = \frac{\ln[\alpha\beta t + 1]}{\beta}$	q_t, adsorption capacity at time $t = t$ [mg g^{-1}]; β, desorption constant of Elovich model [g mg^{-1}]; t, time [min]; α, initial sorption rate of Elovich model [mg g^{-1} min^{-1}]	[25]
Fractional power	$q_t = k_p t^{\nu}$	k_p, fractional power model constant [mg g^{-1}]; ν, rate constant of fractional power model [min^{-1}]	[25]
Pseudo-first-order	$\frac{dq_t}{dt} = k_1(q_{e1} - q_t)$	q_{e1}, adsorption capacity at equilibrium [mg g^{-1}]; q_t, adsorption capacity [mg g^{-1}] at time t (min); k_1, rate constant of the model [min^{-1}]	[26]
Pseudo-second-order	$\frac{dq_t}{dt} = k_2(q_{e2} - q_t)^2$	k_2, rate constant of pseudo-second-order model [g mg^{-1} min^{-1}]; q_{e2}, adsorption capacity at equilibrium [mg g^{-1}]	[26]
	$h = k_2 q_e^2$	h, initial adsorption rate [mg g^{-1} min^{-1}]	
Isotherm models			
	$q_e = \frac{q_{\max} b C_e}{1 + bC_e}$	$q_{\max}$, maximum adsorption capacity [mg g^{-1}]; q_e, adsorption capacity at equilibrium [mg g^{-1}]; b, Langmuir model constant [L mg^{-1}]; C_e, adsorbate concentration at equilibrium [mg L^{-1}]	[27]
Langmuir	$R_L = \frac{1}{1 + bC_0}$	R_L, Hall separation factor [dimensionless]; C_0, initial concentration of AB80 [mg L^{-1}]	[28]
	$\theta = \frac{bC_0}{1 + bC_0}$	θ, surface coverage [dimensionless]	[28]
Freundlich	$q_e = k_f C_e^{1/n_f}$	k_f, Freundlich model constant [mg g^{-1}] [mg L^{-1}]$^{-1/n_f}$; n_f, Freundlich model constant [dimensionless]	[27]
Halsey	$q_e = \left(\frac{k_H}{C_e}\right)^{1/n_H}$	k_H, Halsey model constant [L g^{-1}]; n_H, Halsey model exponent [dimensionless]	[27]
Dubinin-Radushkevich	$q_e = q_{\max}\exp(-B_D\varepsilon_D^2)$	B_D, adsorption energy constant [mol^2 kJ^{-2}]; ε_D, Polanyi potential [kJ mol^{-1}]	[27]
Sips	$q_e = \frac{q_{\max} b_S C_e^{1/n_S}}{1 + b_S C_e^{1/n_S}}$	b_S, affinity coefficient [mg L^{-1}]$^{-1/n_S}$; n_S, Sips model constant [dimensionless]	[27]
Redlich-Peterson	$q_e = \frac{k_{RP} C_e}{1 + a_{RP} C_e^{\beta_{RP}}}$	k_{RP} [L g^{-1}] and a_{RP} [L mg^{-1}]$^{\beta_{RP}}$, Redlich-Peterson model constants; β_{RP}, Redlich-Peterson model exponent [dimensionless]	[27]
Toth	$q_e = \frac{q_{\max} b_T C_e}{\left[1 + (b_T C_e)^{1/n_T}\right]^{n_T}}$	b_T, Toth model constant [L mg^{-1}]; n_T, Toth model constant [dimensionless]	[27]
Khan	$q_e = \frac{q_{\max} b_K C_e}{(1 + b_K C_e)^{a_K}}$	b_K, Khan model constant; a_K, Khan isotherm model exponent	[27]
Koble-Corrigan	$q_e = \frac{\alpha_{CK} C_e^{n_{CK}}}{1 + \beta_{CK} C_e^{n_{CK}}}$	α_{CK} [L$^{n_{CK}}$ mg$^{1-n_{CK}}$ g] and β_{CK} [L mg^{-1}]$^{n_{CK}}$, Koble-Corrigan model constants; n_{CK}, Koble-Corrigan isotherm exponent	[29]
Fritz-Schluender	$q_e = \frac{A_{FS} C_e^{\alpha_{FS}}}{1 + B_{FS} C_e^{\beta_{FS}}}$	A_{FS} [mg g^{-1}] [mg L^{-1}]$^{-\alpha_{FS}}$, β_{FS} [mg L^{-1}]$^{\beta_{FS}}$, Fritz-Schluender model constants; α_{FS}, Fritz-Schluender exponent [dimensionless]	[29]
Thermodynamic models			
Arrhenius	$k_2 = A_0\exp^{(-E_A/RT)}$	E_A, activation energy [kJ mol^{-1}]; R, gas constant; A_0, Arrhenius constant	[30]
Eyring-Polányi	$\ln\frac{k_2}{T} = \ln\frac{k_b}{h} + \frac{\Delta S^*}{R} - \frac{\Delta H^*}{RT}$	k_b, Boltzmann constant; ΔS^*, activation entropy change [kJ mol^{-1} K^{-1}]; ΔH^*, activation enthalpy change [kJ mol^{-1}]	[30]
Gibbs free energy	$\Delta G^* = \Delta H^* - T\Delta S^*$	ΔG^*, Gibbs free energy change [kJ mol^{-1}]	[30]

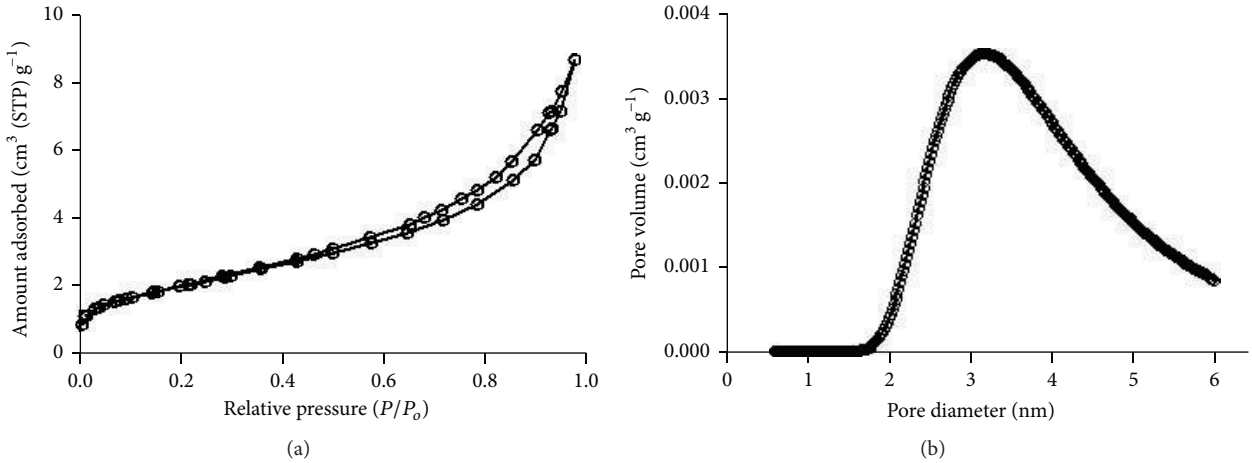

Figure 1: Nitrogen adsorption-desorption isotherm (a) and the corresponding pore size distribution curve (b) for the Cu-TiO_2 sample.

Table 2: Chemical analysis of Cu-TiO_2 composite.

Element	Weight (%)
O	40.21
Ti	52.38
Cu	6.6
S	0.82

7.35 m^2 g^{-1}. As it is evident from Figure 1(b), the Cu-TiO_2 sample has an extended mesopore structure with a total pore volume of 0.011 cm^3 (STP) g^{-1} and an average pore diameter of 3.16 nm.

Field emission scanning electron microscopy (FE-SEM) has been widely used to examine the morphological and surface characteristics of different materials. In the present study, FE-SEM micrographs reveal that Cu-TiO_2 particles have a smooth surface, show round to ovoid shape, and form agglomerates of different morphology (Figures 2(a)–2(c)). This is because small copper oxide particles formed during the annealing process accumulate and grow on the TiO_2 surface, resulting in the formation of agglomerates of different sizes (140–220 nm). Similar results were previously reported by Villanueva-Jaramillo et al. [32] and Hernández et al. [33], who used similar reaction conditions for the preparation of a Cu-TiO_2 composite.

Results from EDS show that the Cu content of Cu-TiO_2 composite was high (6.6% w/w) (Figure 2(d), Table 2). Low sulfur content (0.82% w/w) was detected in the composite, whose presence may be due to the incomplete decomposition of the doping precursor ($CuSO_4$) at 450°C.

The XRD patterns of Cu-TiO_2 are shown in Figure 2(e). The diffraction peaks of both anatase phase and rutile phase of TiO_2 were well defined. In addition, peaks at 2θ of 32.4° and 56.5° were ascribed to diffraction of (110) and (021) planes of CuO, respectively; while the diffraction peak observed at 2θ of 42.3° corresponds to the (200) plane of Cu_2O. The presence of copper oxides in the Cu-TiO_2 composite is due to the doping precursor ($CuSO_4$) and to the composite synthesis methodology used in the present work. Under the conditions of the present synthesis method, Cu from $CuSO_4$ precipitates as $Cu(OH)_2$ on TiO_2 under alkaline conditions (pH 9.0), which subsequently transforms into copper oxides on annealing at 450°C.

Figure 2(f) shows that the optical band gap (E_g) shifts from 3.18 eV (390 nm) for the undoped TiO_2 to 2.3 eV (539 nm) for the Cu-doped TiO_2. The observed value of band gap for the Cu-TiO_2 composite is similar to that reported (2.83 eV) by Karunakaran et al. [34] for a Cu-TiO_2 composite capable of degrading organic compounds under visible light irradiation.

In the present work, the photocatalytic performance of Cu-doped TiO_2 and undoped TiO_2 composites was tested by degrading 10 mg AB80 L^{-1} under visible light irradiation. The Cu-doped TiO_2 exhibited a degradation efficiency of 70%, whereas the undoped TiO_2 was not capable of degrading the AB80 dye over a 4 h period (data not shown). The better photocatalytic performance of Cu-TiO_2 can be attributed to the following reasons. As the valence of Cu^{2+} ions is less than that of Ti^{4+}, doping with Cu induces oxygen vacancies, which act as the active sites for water dissociation on the surface of TiO_2 and can also act as charge carriers of holes (positive effect), while facilitating the separation of photoinduced electron-hole pairs. Oxygen vacancies can efficiently transfer photoinduced electrons to reduce the recombination of electron-hole pairs and thus enhance the visible light photocatalytic activity of TiO_2 [15, 35, 36]. Furthermore, the Cu-TiO_2 composite exhibits an enhanced light harvest in both the UV and visible light regions, enabling much more light energy to be utilized for photocatalysis [36].

3.2. Determination of Point of Zero Charge (PZC). The surface charge of Cu-TiO_2 highly depends on the solution pH and affects its adsorption capacity and consequently the photocatalytic oxidation. The pH at which the net charge of the adsorbent is zero is known as the point of zero charge (PZC) or isoelectric point, and it can be used to assess the adsorbent surface charge qualitatively [19].

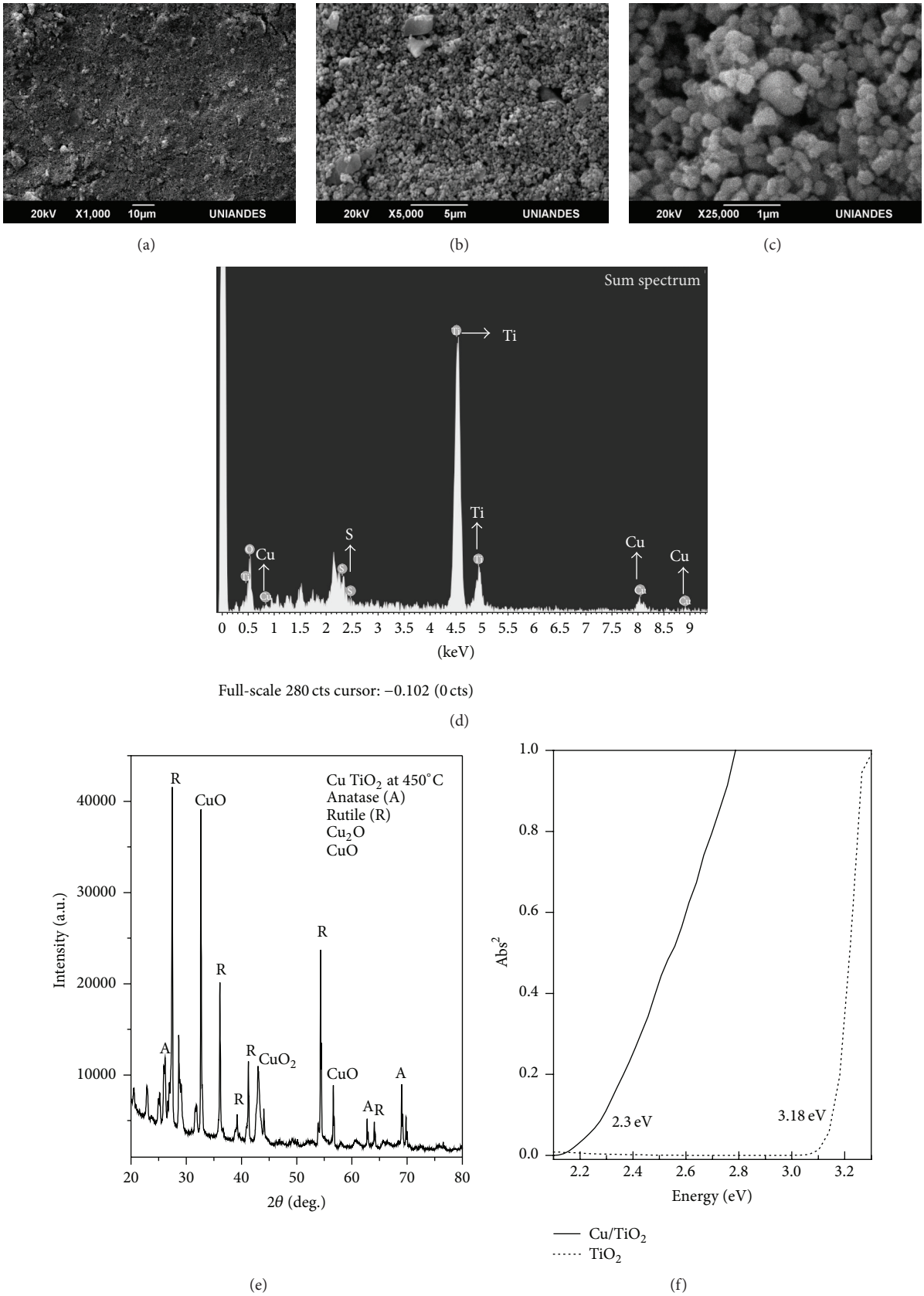

Figure 2: Characterization of Cu-TiO_2 composite by FE-SEM (a–c), EDS (d), XRD (e), and UV-Vis scanning (f).

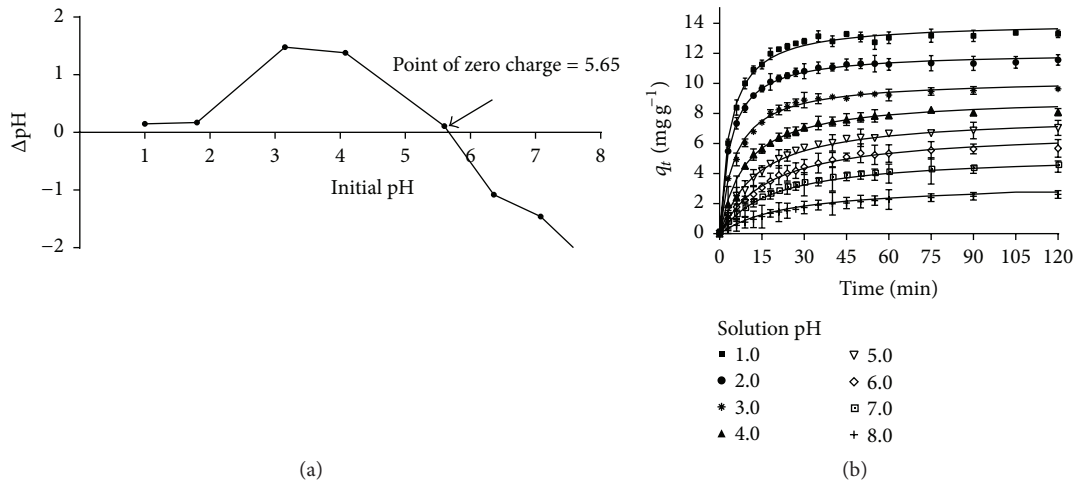

Figure 3: (a) Determination of point of zero charge of Cu-TiO_2. (b) Effect of solution pH on the AB80 adsorption capacity of Cu-TiO_2.

The PZC of Cu-TiO_2 was found to be 5.65 (Figure 3(a)). Hence, for solution pH values lower than 5.65, the surface of the Cu-TiO_2 becomes positively charged, and the opposite occurs for solutions with pH higher than 5.65.

The PZC of Cu-TiO_2 is different from that reported for TiO_2, which ranges from 6.2 to 6.9 [19], and this can be ascribed to the addition of the doping metal [Cu(II)]. This result is in agreement with other studies that have shown that PZC depends on the chemical composition of both the particle surfaces and the surrounding solvent [19, 37, 38].

3.3. Effect of pH on AB80 Adsorption Kinetics. The pH of a dye solution is a key environmental parameter in the adsorption process because it affects the surface charge of the adsorbent, the ionization state of the dye molecule, and the solubility of dyes in the aqueous solution [39, 40].

Figure 3(b) shows the variations in AB80 adsorption capacity of Cu-TiO_2 with respect to contact time at different pH values ranging from 1.0 to 8.0. It is evident that the adsorption of AB80 onto the Cu-TiO_2 composite showed strong pH dependence. The capacity of Cu-TiO_2 for adsorbing AB80 increased as the solution pH decreased and reached its highest level at pH 1.0. A similar behavior has been observed in the adsorption of reactive red 198 on TiO_2 [41], acid green 25 on alginate-TiO_2 [42], and N719 on TiO_2 [43].

The interpretation of the effect of solution pH on AB80 adsorption onto Cu-TiO_2 can be well-explained with the help of the PZC of Cu-TiO_2. For AB80 solutions with pH < PZC (i.e., below pH 5.65), the net surface charge of Cu-TiO_2 is positive due to the adsorption of protons (H^+ and H_3O^+), which favored the adsorption of anionic AB80 due to electrostatic attraction. In contrast, the decrease in AB80 adsorption capacity observed at pH values of dye solution > PZC may be due to the electrostatic repulsion between the negatively charged Cu-TiO_2 surface and the anionic AB80 dye and also to the competition between OH^- ions and AB80 molecules for occupancy of the binding sites [4, 42, 44]. However, the Cu-TiO_2 composite could still adsorb AB80 dye at higher solution pH, which indicates that the electrostatic mechanism was not the only mechanism for AB80 adsorption in this system. Cu-TiO_2 could also adsorb AB80 dye molecules via hydrogen bonding and hydrophobic mechanisms [45]. Nevertheless, the AB80 adsorption capacity of Cu-TiO_2 at solution pH values < PZC was much higher than that obtained at pH > PZC, suggesting that the electrostatic interaction was the main mechanism.

The optimal solution pH for AB80 adsorption onto the Cu-TiO_2 composite was 1.0, and this pH was therefore used in further experiments.

3.4. Influence of Contact Time and Initial AB80 Concentration on Dye Adsorption. Figure 4 shows the variations in AB80 adsorption capacity with respect to adsorption time at different initial AB80 concentrations ranging from 10 to 150 mg L^{-1}. At all of the tested initial dye concentrations, AB80 adsorption capacity gradually rose as experimental adsorption time passed until adsorption capacity reached a maximum constant value that corresponded to the equilibrium adsorption capacity (exp q_e) value. Likewise, regardless of initial AB80 concentration, the rate of the AB80 adsorption process was fast during the first 15 min of contact time, and this may be because a large number of positively charged active sites are available for adsorption of AB80 on the Cu-TiO_2 surface. Thereafter, AB80 adsorption rate decreased gradually until the dynamic equilibrium was reached within the first 60 min; at this point, the active Cu-TiO_2 sites were all occupied by AB80 molecules. The short duration of the present experiments indicates that the AB80 adsorption is kinetics-controlled rather than diffusion-controlled process [19]. It is clear from Figure 4 that the AB80 adsorption capacity increased as the initial dye concentration increased from 10 to 90 mg L^{-1}. This effect may be due to the higher availability of AB80 molecules in aqueous solution, which enhanced the interaction between the AB80 dye molecules and the Cu-TiO_2 composite. Higher AB80 concentration also increases the driving force of the dye concentration gradient to overcome the resistance to the mass transfer of AB80 between the aqueous phase and the solid phase of Cu-TiO_2, which

Table 3: Effect of the initial AB80 concentration on the kinetics parameters of the models for AB80 adsorption onto Cu-TiO_2.

(a)

C_0 [mg L^{-1}]	exp q_e [mg g^{-1}]	exp t_e [min]	Elovich					Fractional power				
			α [mg g^{-1} min^{-1}]	β [g mg^{-1}]	r^2	SSE	RMSE	k_p [mg min^{-1}]	ν [min^{-1}]	r^2	SSE	RMSE
10	3.395	21	0.803 ± 0.290	1.310 ± 0.170	0.978	0.320	0.146	1.010 ± 0.20	0.277 ± 0.053	0.95	0.752	0.224
20	7.725	21	11.50 ± 6.260	0.850 ± 0.098	0.983	1.063	0.250	3.610 ± 0.40	0.175 ± 0.029	0.96	2.087	0.350
30	11.60	21	2.842 ± 1.320	0.380 ± 0.063	0.957	8.664	0.675	3.590 ± 0.84	0.269 ± 0.061	0.91	17.86	0.969
40	12.67	24	8.587 ± 5.740	0.435 ± 0.074	0.953	9.929	0.722	5.330 ± 0.97	0.204 ± 0.048	0.92	16.76	0.939
50	14.00	27	21.43 ± 20.30	0.473 ± 0.090	0.946	12.46	0.809	6.740 ± 1.13	0.168 ± 0.045	0.91	18.77	0.994
70	17.06	30	47.79 ± 46.21	0.468 ± 0.813	0.963	10.26	0.735	8.280 ± 1.08	0.149 ± 0.035	0.94	15.55	0.905
90	18.46	30	32.61 ± 36.42	0.356 ± 0.803	0.932	29.03	1.236	9.340 ± 1.60	0.163 ± 0.048	0.90	41.34	1.475
120	18.71	40	77.24 ± 117.1	0.422 ± 0.107	0.927	27.62	1.206	10.10 ± 1.64	0.139 ± 0.005	0.90	35.94	1.375
150	19.43	40	74.65 ± 92.25	0.412 ± 0.080	0.949	19.56	1.015	10.14 ± 1.40	0.142 ± 0.039	0.93	26.95	1.191

(b)

C_0 [mg L^{-1}]	Pseudo-first-order					Pseudo-second-order					
	k_1 [min^{-1}]	q_{e1} [mg g^{-1}]	r^2	SSE	RMSE	k_2 [g mg^{-1} min^{-1}]	q_{e2} [mg g^{-1}]	h [mg g^{-1} min^{-1}]	r^2	SSE	RMSE
10	0.071 ± 0.012	3.278 ± 0.154	0.971	0.425	0.168	0.028 ± 0.004	3.782 ± 0.13	0.400	0.991	0.135	0.09
20	0.135 ± 0.135	7.305 ± 0.306	0.944	3.622	0.462	0.022 ± 0.004	8.016 ± 0.19	1.414	0.990	0.630	0.19
30	0.076 ± 0.005	11.19 ± 0.210	0.993	1.269	1.384	0.015 ± 0.002	12.74 ± 0.25	2.435	0.996	0.296	0.47
40	0.105 ± 0.093	12.39 ± 0.280	0.984	2.424	3.411	0.014± 0.0004	13.83 ± 0.31	2.678	0.992	1.661	0.29
50	0.134 ± 0.013	13.32 ± 0.250	0.987	1.403	3.080	0.012 ± 0.002	14.91 ± 0.23	2.668	0.995	1.153	0.24
70	0.165 ± 0.330	14.97 ± 0.022	0.976	6.476	0.584	0.012 ± 1.000	17.71 ± 0.23	3.763	0.997	1.141	0.25
90	0.145 ± 0.012	17.99 ± 0.270	0.990	4.029	0.461	0.011 ± 0.002	19.72 ± 0.41	4.278	0.994	3.708	0.44
120	0.177 ± 0.017	17.47 ± 0.270	0.989	4.235	0.472	0.011 ± 0.002	19.80 ± 0.37	4.312	0.994	3.499	0.43
150	0.175 ± 0.022	17.74 ± 0.360	0.980	7.540	0.630	0.011 ± 0.001	19.83 ± 0.30	4.326	0.995	2.171	0.33

increases the probability of collision between AB80 molecules and active Cu-TiO_2 sites and thus leads to enhanced adsorption capacity [4, 45–48]. In contrast, at initial AB80 concentrations between 90 and 150 mg L^{-1}, the adsorption capacities were very similar; this was probably due to the saturation of the adsorption active sites. It is apparent from the above results that saturation of the Cu-TiO_2 surface with AB80 molecules is dependent on initial dye concentration.

The contact time required to reach equilibrium is an important parameter from a practical and economical point of view. As seen in Table 3, the equilibrium time (exp t_e) increased from 21 to 40 min with increasing initial AB80 concentration from 10 to 150 mg L^{-1}, and this increase was observed because Cu-TiO_2 adsorbed larger amounts of AB80 as the initial dye concentration increased.

3.5. Effect of Temperature on AB80 Adsorption. Figure 5 shows that, at the two initial AB80 concentrations (30 and 120 mg L^{-1}) tested, the Cu-TiO_2 AB80 adsorption capacity and rate increased with rising temperature of the adsorption system from 25 to 60°C, and consequently the time required to reach equilibrium decreased as the temperature increased

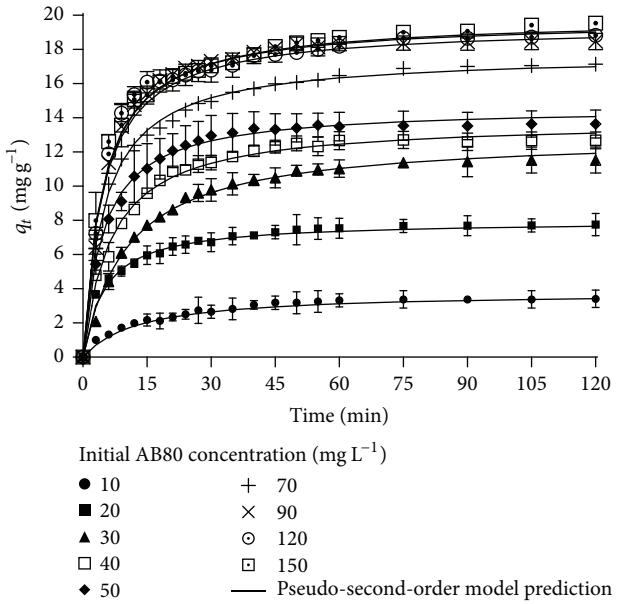

Figure 4: Influence of initial AB80 concentration on the AB80 adsorption capacity of Cu-TiO_2.

Table 4: Kinetics model parameters for AB80 adsorption onto Cu-TiO_2 at different temperatures.

(a)

C_0 [mg L^{-1}]	T [°C]	exp q_e [mg g^{-1}]	exp t_e [min]	Elovich					Fractional power				
				α [mg g^{-1} min^{-1}]	β [g mg^{-1}]	r^2	SSE	RMSE	k_p [mg min^{-1}]	ν [min^{-1}]	r^2	SSE	RMSE
30	25	11.5	35	2.816 ± 1.290	0.381 ± 0.062	0.959	8.435	0.666	3.581 ± 0.832	0.270 ± 0.060	0.914	17.59	0.962
	40	13.1	30	7.927 ± 5.430	0.412 ± 0.075	0.948	12.19	0.801	5.378 ± 0.941	0.209 ± 0.052	0.912	20.52	1.039
	50	14.8	24	12.17 ± 9.820	0.392 ± 0.076	0.942	16.59	0.934	6.483 ± 1.254	0.193 ± 0.051	0.907	26.37	1.178
	60	15.9	21	28.49 ± 27.1	0.418 ± 0.079	0.950	15.15	0.893	7.948 ± 1.246	0.165 ± 0.042	0.926	22.43	1.086
120	25	18.6	45	3.392 ± 1.350	0.219 ± 0.035	0.964	20.28	1.033	5.089 ± 1.237	0.297 ± 0.062	0.918	45.08	1.540
	40	20.8	24	8.969 ± 5.521	0.246 ± 0.044	0.949	30.9	1.275	7.736 ± 1.641	0.228 ± 0.056	0.909	54.32	1.691
	50	22.7	20	16.35 ± 12.53	0.243 ± 0.047	0.942	41.15	1.472	9.804 ± 1.946	0.201± 0.052	0.907	65.92	1.863
	60	25.4	18	157.1 ± 218.0	0.317 ± 0.069	0.949	36.08	0.947	14.59 ± 1.990	0.132 ± 0.037	0.932	48.37	1.596

(b)

C_0 [mg L^{-1}]	T [°C]	Pseudo-first-order					Pseudo-second-order					
		k_1 [min^{-1}]	q_{e1} [mg g^{-1}]	r^2	SSE	RMSE	k_2 [g mg^{-1} min^{-1}]	q_{e2} [mg g^{-1}]	h [mg g^{-1} min^{-1}]	r^2	SSE	RMSE
30	25	0.075 ± 0.005	11.21 ± 0.22	0.992	1.466	0.278	0.007 ± 0.001	12.97 ± 0.32	1.177	0.994	1.200	0.251
	40	0.107 ± 0.009	12.71 ± 0.24	0.989	2.534	0.365	0.011 ± 0.001	14.27 ± 0.32	2.240	0.992	1.811	0.309
	50	0.118 ± 0.008	14.25 ± 0.22	0.992	2.183	0.339	0.012 ± 0.001	15.86 ± 0.32	3.018	0.995	2.014	0.326
	60	0.139 ± 0.016	15.44 ± 0.35	0.979	6.189	0.571	0.013 ± 0.001	16.90 ± 0.34	3.713	0.992	2.497	0.363
120	25	0.068 ± 0.005	18.02 ± 0.39	0.992	4.381	0.480	0.004 ± 0.001	21.19 ± 0.01	1.796	0.996	3.773	0.446
	40	0.096 ± 0.007	19.88 ± 0.37	0.991	5.428	0.535	0.006 ± 0.001	22.54 ± 0.59	3.048	0.994	5.213	0.524
	50	0.110 ± 0.009	22.32 ± 0.39	0.991	7.712	0.694	0.008 ± 0.001	24.91 ± 0.61	4.964	0.994	6.695	0.594
	60	0.187 ± 0.020	24.54 ± 0.40	0.987	9.586	0.710	0.012 ± 0.001	26.47 ± 0.31	8.408	0.996	2.689	0.376

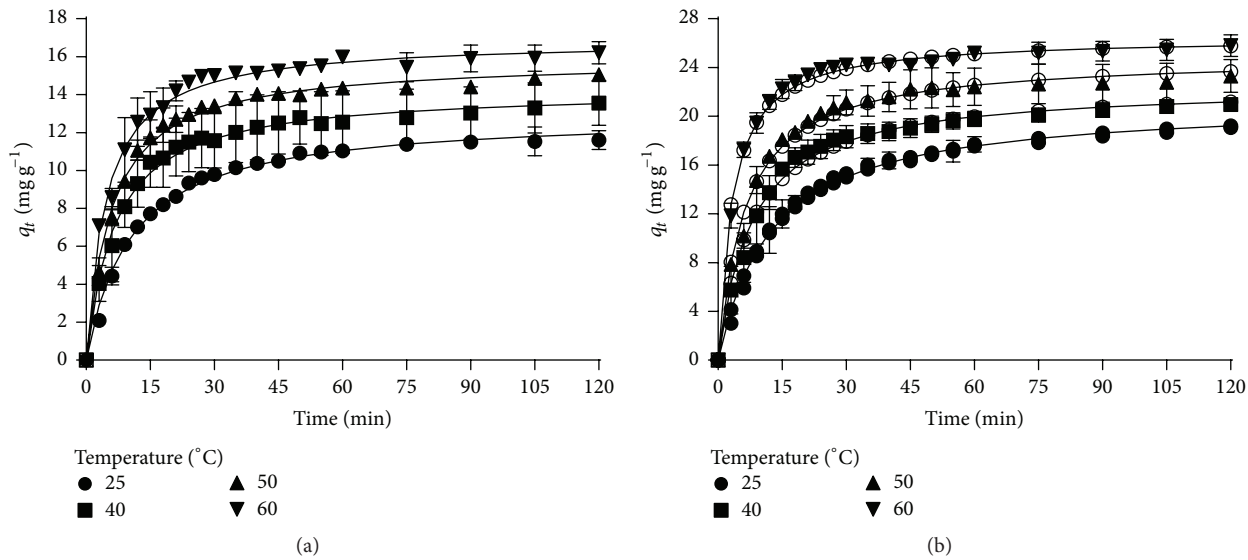

Figure 5: Kinetics of AB80 adsorption onto Cu-TiO_2 at different temperatures. Initial AB80 concentration: (a) 30 mg L^{-1}; (b) 120 mg L^{-1}.

(Table 4). These results indicate that the adsorption process was endothermic in nature and that a chemical reaction between AB80 molecules and the Cu-TiO_2 surface is involved in the adsorption process [49].

The larger AB80 adsorption capacity and rate at higher temperature may be due to the following: (1) an increase in kinetic energy, which facilitates the diffusion of dye molecules to the active Cu-TiO_2 adsorption sites, (2) a decrease in

the thickness of the boundary layer surrounding the adsorbent, which, in turn, decreases the mass transfer resistance of dye molecules in the boundary layer, and (3) an increase in the Cu-TiO_2 surface activity [44, 50].

3.6. Kinetics Modeling of AB80 Adsorption onto Cu-TiO_2. Kinetics profiles of AB80 adsorption were modeled to determine the rate-controlling mechanisms involved in the adsorption process. For this purpose, the Elovich, fractional power, pseudo-first-order, and pseudo-second-order kinetics models were used to analyze the experimental adsorption data at different initial AB80 concentrations and temperatures.

Tables 3 and 4 list the experimental equilibrium adsorption capacity ($\exp q_e$), the parameter values of the Elovich (α and β), fractional power (k_p and ν), pseudo-first-order (k_1 and q_{e1}), and pseudo-second-order (k_2, q_{e2}, and h) kinetics models for AB80 adsorption at initial AB80 concentrations from 10 to 150 mg L^{-1}, and temperatures from 25 to 60°C, together with the corresponding r^2, RMSE, SSE, and 95% confidence interval values.

The determination coefficients were higher with the pseudo-second-order model, and the RMSE and SSE values were lower than those obtained with the Elovich, fractional power, pseudo-first-order, and pseudo-second-order models, which denotes a good agreement of experimental data with the pseudo-second-order model for the initial AB80 concentrations and temperatures tested. Moreover, the equilibrium adsorption capacity (q_{e2}) values predicted by the pseudo-second-order kinetics model agree very well with the experimental data ($\exp q_e$). Additionally, the pseudo-second-order model successfully described the kinetics profiles of AB80 adsorption from aqueous solutions onto Cu-TiO_2 at the assayed initial AB80 concentrations and temperatures (continuous lines in Figures 4 and 5). According to these results, the AB80 adsorption kinetics on Cu-TiO_2 are best described by the pseudo-second-order model, which is based on the assumption that the rate-limiting step may be chemical sorption or chemisorption involving valence forces through the sharing or exchange of electrons between the adsorbent (Cu-TiO_2) and sorbate (AB80) [19]. This result is in agreement with that reported by Bourikas et al. [51], who proposed that the adsorption of sulfonic acid dyes on TiO_2 occurs via the sulfonic group of the azo dye through the formation of a bidentate inner sphere surface complex.

The pseudo-second-order model is also the most suitable to describe the adsorption kinetics of reactive red 195 on TiO_2 [19], C.I. basic blue 41 on N,F-codoped flower-like TiO_2 [12], direct red 80 and acid green 25 on sodium alginate-TiO_2 [42], and methylene blue on polypyrrole-TiO_2 [45], among others.

Results also show that the pseudo-second-order model rate constant (k_2) was strongly dependent on the initial AB80 concentration and temperature. The rate constant k_2 decreased as the initial AB80 concentration increased (Table 3), which may be observed because, at higher initial AB80 concentrations, the Cu-TiO_2 composite adsorbed larger amounts of AB80 and therefore required longer contact times to reach equilibrium. This trend has also been reported for other adsorption systems [19, 52, 53].

Furthermore, at the two initial AB80 concentrations assayed, k_2 values increased as the temperature of the adsorption system rose (Table 4). This can be explained on the basis of increases in the interactions between AB80 molecules and the Cu-TiO_2 composite with increasing temperature, which confirms that the AB80 adsorption rate is faster at higher temperatures, as well as confirming the endothermic nature of the adsorption process [4, 44].

Likewise, the initial adsorption rate (h) tended to increase as the initial AB80 concentration (Table 3) and temperature (Table 4) increased, which confirms that the initial AB80 adsorption rate increased with the rise in initial dye concentration and temperature.

3.7. Adsorption Isotherm Modeling of AB80 onto Cu-TiO_2. Figure 6 presents the equilibrium isotherm for AB80 adsorption onto Cu-TiO_2 at pH 1.0 and 25°C. It is evident that the equilibrium adsorption capacity (q_e) increased gradually with the increase in the equilibrium AB80 concentration (C_e) until it reached a maximum constant value, of approximately 19.78 mg g^{-1}. The shape of the AB80 adsorption isotherm indicates that as active adsorption sites of Cu-TiO_2 are occupied, it becomes more difficult for AB80 molecules to find available Cu-TiO_2 adsorption sites; that is, it suggests a progressive saturation of the Cu-TiO_2 composite [53].

The shape and initial slope of the AB80 adsorption isotherm belong to the type L isotherm of the Giles classification [54], which is generally associated with the adsorption of a monomolecular layer of adsorbate with a minimum competition for the solvent, a high affinity between adsorbate and adsorbent, and the occurrence of a chemisorption reaction between adsorbate and adsorbent [55].

In the present study, the experimental equilibrium data of AB80 adsorption onto Cu-TiO_2 were analyzed using two- (Langmuir, Freundlich, Halsey, and Dubinin-Radushkevich), three- (Koble-Corrigan, Sips, Redlich-Peterson, Toth, and Khan), and four-parameter (Fritz-Schluender) isotherm models. Figure 6 shows the predicted fittings of the isotherm models to the experimental data, and Table 5 shows the model parameter values along with 95% confidence intervals, as well as r^2, SSE, and RMSE values.

The Langmuir model was found to have the best fit to the experimental data of AB80 adsorption among the two-parameter isotherm models, with a high determination coefficient ($r^2 = 0.994$) and low RMSE (0.259) and SSE (0.203) values. In contrast, the Freundlich, Halsey, and Dubinin-Radushkevich isotherm models were unable to describe the experimental equilibrium data, having lower coefficients of determination and higher RMSE and SSE values than those of the Langmuir model.

All of the three-parameter models (Koble-Corrigan, Sips, Redlich-Peterson, Toth, and Khan) as well as the four-parameter (Fritz-Schluender) model had high coefficients of determination and lower RMSE and SSE values. However, the 95% confidence intervals of the Koble-Corrigan, Redlich-Peterson, Khan, and Fritz-Schluender isotherm parameters were wider than those of the Langmuir model.

Table 5: Isotherm constants of two-, three-, and four-parameter models for AB80 adsorption onto Cu-TiO_2.

Two-parameter models	
Langmuir	
b [L mg^{-1}]	0.0465 ± 0.009
q_{max} [mg g^{-1}]	22.23 ± 1.87
r^2	0.994
RMSE	0.259
SSE	0.203
Freundlich	
k_f [mg g^{-1}] [mg L^{-1}]$^{-1/n_f}$	3.038 ± 1.971
n_f	2.514 ± 0.953
r^2	0.931
RMSE	1.71
SSE	14.62
Halsey	
k_H [L g^{-1}]	16.35 ± 43.79
n_H	2.514 ± 0.953
r^2	0.931
RMSE	1.71
SSE	14.62
Dubinin-Radushkevich	
B_D [mol^2 kJ^{-2}]	26.36
q_{max} [mg g^{-1}]	18.14 ± 6.23
r^2	0.89
RMSE	2.136
SSE	22.81
Three-parameter models	
Koble-Corrigan	
α_{CK} [L$^{n_{CK}}$ mg$^{1-n_{CK}}$ g]	1
β_{CK} [L mg^{-1}]$^{n_{CK}}$	0.041 ± 0.05
n_{CK}	0.973 ± 0.75
r^2	0.992
RMSE	0.589
SSE	1.734
Sips	
b_S [mg L^{-1}]$^{-1/n_S}$	0.021 ± 0.007
n_S	0.9802 ± 0.014
q_{max} [mg g^{-1}]	21.59 ± 1.05
r^2	0.998
RMSE	0.205
SSE	0.168
Redlich-Peterson	
a_{RP} [L mg^{-1}]$^{\beta_{RP}}$	0.01223 ± 0.013
β_{RP}	1.183 ± 0.805
k_{RP} [L g^{-1}]	0.8462 ± 0.579
r^2	0.997
RMSE	0.3163
SSE	0.4002
Toth	
b_T [L mg^{-1}]	0.1
n_T	1.345 ± 0.149
q_{max} [mg g^{-1}]	12.55 ± 2.15
r^2	0.9823
RMSE	0.7904
SSE	3.123
Khan	
b_K	0.018 ± 0.034
a_K	1.353 ± 0.673
q_{max} [mg g^{-1}]	42.65 ± 39.88
r^2	0.996
RMSE	0.362
SSE	0.525
Four-parameter model	
Fritz-Schluender	
A_{FS} [mg g^{-1}] [mg L^{-1}]$^{-\alpha_{FS}}$	0.407 ± 0.529
B_{FS} [mg L^{-1}]$^{-\beta_{FS}}$	0.0226 ± 0.043
α_{FS}	1.336 ± 1.666
β_{FS}	1.302 ± 0.452
r^2	0.999
RMSE	0.233
SSE	0.161

These models were therefore not suitable to describe the experimental isotherm. Furthermore, the maximum AB80 adsorption capacities (q_{max}) predicted by the Toth and Khan models were substantially lower and higher, respectively, than that found experimentally (19.78 mg g^{-1}), and consequently these isotherm models did not properly describe the adsorption equilibrium of AB80 by Cu-TiO_2. Moreover, the Sips model rendered a coefficient of determination, RMSE and SSE values, and 95% confidence interval similar to those of the Langmuir model, and consequently neither the Langmuir model nor the Sips model showed any added advantage (Table 5). However, the exponent value of the Sips model was close to 1.0, with which value this isotherm model is reduced to the Langmuir model [4]. Based on these results, the Langmuir model agrees best with the experimental equilibrium data for the adsorption of AB80 by Cu-TiO_2. The applicability of the Langmuir model to the adsorption system under investigation suggests that the AB80 adsorption behavior of Cu-TiO_2 follows a homogeneous monolayer chemisorption process [56]. The Langmuir model also fitted the equilibrium data of AB80 adsorption by TiO_2 [57].

The Langmuir model has great practical importance because it is simpler than the three- and four-parameter isotherm models and can consequently be applied and interpreted more easily and may therefore be especially useful for designing and scaling up adsorption processes [4].

The Langmuir model predicted a maximum AB80 adsorption capacity of 22.23 mg g^{-1}, which approximates the experimental AB80 adsorption capacity at equilibrium (19.78 mg g^{-1}). The AB80 adsorption capacity of Cu-TiO_2 is similar to that reported for TiO_2 at pH 6.0 and higher than that found at pH 9.0 [57].

Furthermore, the Langmuir equilibrium affinity constant (b) was 0.0465 L mg^{-1} (Table 5), and this was used to calculate the dimensionless Hall separation factor (R_L) and the surface coverage (θ), which are helpful to predict whether the adsorption system is "favorable" or "unfavorable" and to predict the fraction of Cu-TiO_2 adsorption sites occupied by AB80 molecules at equilibrium, respectively. Figure 7(a) shows that

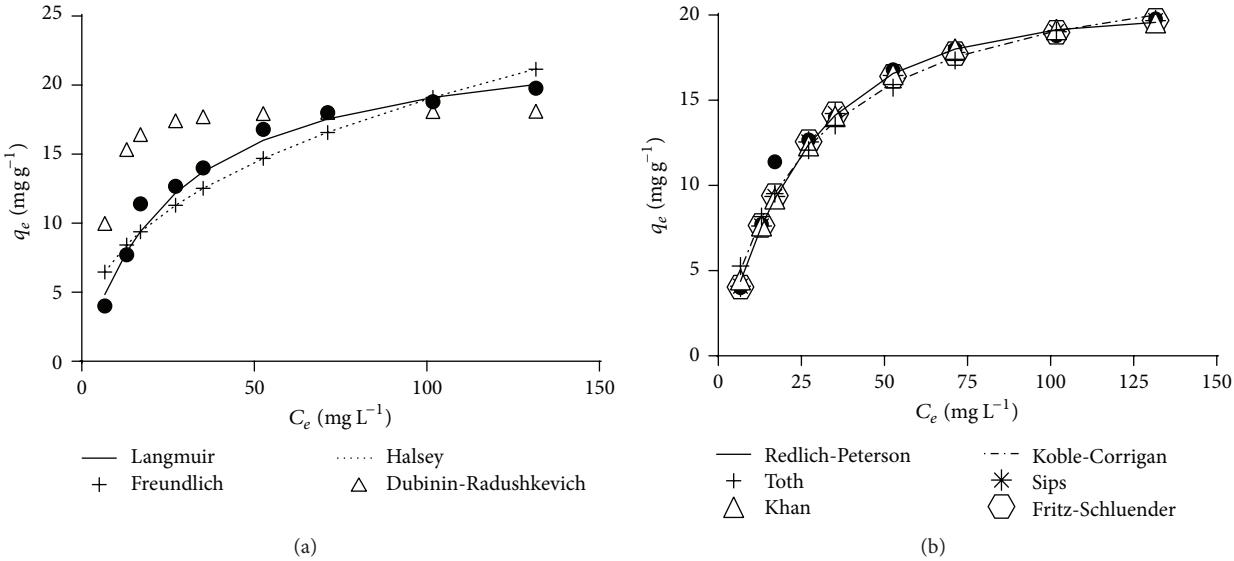

FIGURE 6: Experimental (●) isotherm data and calculated isotherm data derived from two-parameter (a) and three- and four-parameter (b) models for AB80 adsorption by Cu-TiO_2.

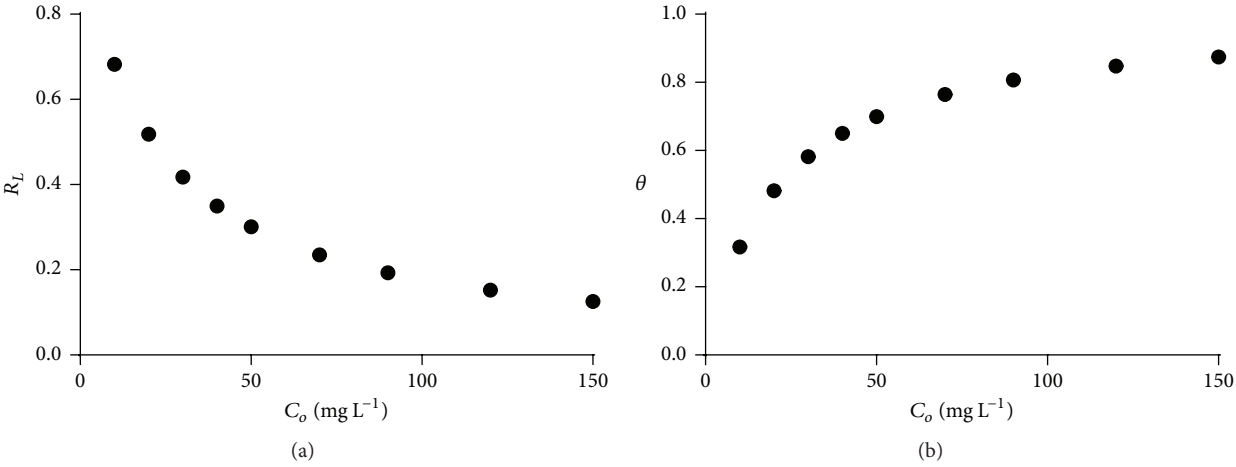

FIGURE 7: Dependence of separation factor (a) and surface coverage (b) on initial AB80 concentration.

the Hall separation factor decreased as the initial AB80 concentration increased, which indicates that AB80 adsorption is enhanced as the starting concentration of the dye in solution increases. Furthermore, all R_L values obtained were between 0 and 1.0, indicating that the AB80 adsorption by Cu-TiO_2 was favorable. Figure 7(b) shows that the surface coverage tends to approach unity with an increase in initial AB80 concentration, which indicates that the Cu-TiO_2 surface was almost completely covered with a monomolecular layer of AB80 molecules at the higher AB80 concentrations.

To the best of our knowledge, no previous research has been reported on AB80 adsorption by doped TiO_2.

3.8. AB80 Adsorption Thermodynamics. Thermodynamic studies for the present adsorption of AB80 onto Cu-TiO_2 were undertaken to elucidate the mechanism involved in and the feasibility of the AB80 adsorption process. Different relevant thermodynamic parameters, such as the Arrhenius activation energy (E_A), activation enthalpy change (ΔH^*), activation entropy change (ΔS^*), and free energy change (ΔG^*), were estimated, and the results are reported in Table 6.

The values of E_A were found to be 12.75 and 24.32 kJ mol^{-1} when initial AB80 concentrations of 30 and 120 mg L^{-1} were used, respectively. The magnitude of E_A is commonly used to obtain information regarding whether the adsorption process is physical (physisorption) or chemical (chemisorption). E_A value for physical adsorption is usually not higher than 4.184 kJ mol^{-1}, whereas for chemical adsorption it is between 8.4 and 83.7 kJ mol^{-1} [50]. Therefore, Cu-TiO_2 adsorbs AB80 molecules by a chemical adsorption reaction, which agrees with the results of the kinetics and isotherm experiments described above.

ΔH^* values were positive (10.17 and 21.71 kJ mol^{-1}) at the two initial AB80 concentrations tested (30 and 120 mg L^{-1}),

Table 6: Thermodynamic parameters for the adsorption of AB80 onto Cu-TiO_2.

C_0 [mg L^{-1}]	T [°C]	ΔG^* [kJ mol^{-1}]	E_A [kJ mol^{-1}]	A_0 [g mg^{-1} min^{-1}]	ΔS^* [kJ mol^{-1} K^{-1}]	ΔH^* [kJ mol^{-1}]
30	25	28.036	12.75	1.30	−0.06	10.17
	40	28.935				
	50	29.534				
	60	30.133				
120	25	29.879	24.32	65.67	−0.027	21.71
	40	30.291				
	50	30.565				
	60	30.839				

which further confirms that the AB80 adsorption reaction is endothermic. The values of ΔS^* were −0.06 and −0.027 kJ mol^{-1} K^{-1} at initial AB80 concentrations of 30 and 120 mg L^{-1}, respectively. The negative ΔS^* values indicate the association of AB80 molecules with active Cu-TiO_2 sites, which leads to the formation of a stable chemical complex on the Cu-TiO_2 surface. These values also indicate that no significant change occurs in the internal structure of the adsorbent during the adsorption process [30, 58]. This also confirmed the affinity of Cu-TiO_2 for AB80 [39].

Moreover, at all assayed initial AB80 concentrations and temperatures, ΔG^* values were positive (28.04–30.84 kJ mol^{-1}), which indicated that the adsorption process of AB80 onto the active adsorption sites offered by Cu-TiO_2 was not spontaneous in nature and therefore needs to be driven by an outside source of energy [4].

4. Conclusions

A Cu-TiO_2 photocatalyst was synthesized and characterized by X-ray diffraction (XRD), field emission scanning electron microscopy (FE-SEM), energy dispersive X-ray spectroscopy (EDS), and UV-Vis scanning spectroscopy, as well as in terms of specific surface area and pore size distribution; in addition, its ability to remove AB80 from aqueous solutions by adsorption was investigated.

It was found that the modification of TiO_2 with Cu reduced the energy of band gap from 3.18 to 2.3 eV. Both anatase and rutile phases are present in the Cu-TiO_2 composite and the Cu content of this composite is high.

The adsorptive removal of AB80 by Cu-TiO_2 was found to be strongly dependent on the solution pH, initial AB80 concentration, contact time, and temperature. The adsorption behaviors of AB80 on Cu-TiO_2 were described best with the pseudo-second-order kinetics model and the Langmuir isotherm model. Thermodynamic parameters confirmed the endothermic and nonspontaneous nature of the AB80 adsorption process.

Conflict of Interests

The authors declare that there is no conflict of interests regarding the publication of this paper.

Acknowledgments

The authors gratefully acknowledge the support provided by the scientific staff of the Central Laboratories of Spectroscopy, and Biotechnology and Molecular Biology at ENCB-IPN, as well as the financial support provided by the Secretaría de Investigación y Posgrado, IPN, Mexico, and the Pontificia Universidad Javeriana (Research Project 6272), Bogota, Colombia. The CONACyT awarded a graduate scholarship to one of the coauthors (Ingrid Johanna Puentes-Cárdenas). Eliseo Cristiani-Urbina is a holder of grants from COFAA-IPN, EDI-IPN, and SNI-CONACyT.

References

[1] P. Sharma, H. Kaur, M. Sharma, and V. Sahore, "A review on applicability of naturally available adsorbents for the removal of hazardous dyes from aqueous waste," *Environmental Monitoring and Assessment*, vol. 183, no. 1–4, pp. 151–195, 2011.

[2] Y. Du, M. Pei, Y. He, F. Yu, W. Guo, and L. Wang, "Preparation, characterization and application of magnetic Fe_3O_4-CS for the adsorption of orange I from aqueous solutions," *PLoS ONE*, vol. 9, no. 10, Article ID e108647, 2014.

[3] I. Guerrero-Coronilla, L. Morales-Barrera, T. L. Villegas-Garrido, and E. Cristiani-Urbina, "Biosorption of amaranth dye from aqueous solution by roots, leaves, stems and the whole plant of *Eichhornia crassipes*," *Environmental Engineering and Management Journal*, vol. 13, no. 8, pp. 1917–1926, 2014.

[4] I. Guerrero-Coronilla, L. Morales-Barrera, and E. Cristiani-Urbina, "Kinetic, isotherm and thermodynamic studies of amaranth dye biosorption from aqueous solution onto water hyacinth leaves," *Journal of Environmental Management*, vol. 152, pp. 99–108, 2015.

[5] A. Srinivasan and T. Viraraghavan, "Decolorization of dye wastewaters by biosorbents: a review," *Journal of Environmental Management*, vol. 91, no. 10, pp. 1915–1929, 2010.

[6] A. Bhatnagar and A. K. Minocha, "Assessment of the biosorption characteristics of lychee (*Litchi chinensis*) peel waste for the removal of acid blue 25 dye from water," *Environmental Technology*, vol. 31, no. 1, pp. 97–105, 2010.

[7] W. Li, D. Li, Z. Chen et al., "High-efficient degradation of dyes by ZnCdS solid solutions under visible irradiation," *The Journal of Physical Chemistry C*, vol. 38, pp. 14943–14947, 2008.

[8] T. Pauporté and J. Rathouský, "Electrodeposited mesoporous ZnO thin films as efficient photocatalysts for the degradation

of dye pollutants," *Journal of Physical Chemistry C*, vol. 111, no. 21, pp. 7639–7644, 2007.

[9] R. Jain, M. Mathur, S. Sikarwar, and A. Mittal, "Removal of the hazardous dye rhodamine B through photocatalytic and adsorption treatments," *Journal of Environmental Management*, vol. 85, no. 4, pp. 956–964, 2007.

[10] J. Marugán, M. López-Muñoz, R. van Grieken, and J. Aguado, "Photocatalytic decolorization and mineralization of dyes with nanocrystalline TiO_2/SiO_2 materials," *Industrial & Engineering Chemistry Research*, vol. 46, no. 23, pp. 7605–7610, 2007.

[11] L. G. Devi and S. G. Kumar, "Exploring the critical dependence of adsorption of various dyes on the degradation rate using Ln^{3+}-TiO_2 surface under UV/solar light," *Applied Surface Science*, vol. 261, pp. 137–146, 2012.

[12] Y. Jiang, Y. Luo, F. Zhang, L. Guo, and L. Ni, "Equilibrium and kinetic studies of C.I. Basic blue 41 adsorption onto N, F-codoped flower-like TiO_2 microspheres," *Applied Surface Science*, vol. 273, pp. 448–456, 2013.

[13] C. H. Liang, F. B. Li, C. S. Liu, J. L. Lü, and X. G. Wang, "The enhancement of adsorption and photocatalytic activity of rare earth ions doped TiO_2 for the degradation of Orange I," *Dyes and Pigments*, vol. 76, no. 2, pp. 477–484, 2008.

[14] J. Araña, C. G. Rodríguez, O. G. Díaz, J. A. H. Melián, and J. P. Peña, "Role of Cu in the Cu-TiO_2 photocatalytic degradation of dihydroxybenzenes," *Catalysis Today*, vol. 101, no. 3-4, pp. 261–266, 2005.

[15] H. W. P. Carvalho, A. P. L. Batista, P. Hammer, and T. C. Ramalho, "Photocatalytic degradation of methylene blue by TiO_2-Cu thin films: theoretical and experimental study," *Journal of Hazardous Materials*, vol. 184, no. 1–3, pp. 273–280, 2010.

[16] P. Muthirulan, C. Nirmala Devi, and M. Meenakshi Sundaram, "Synchronous role of coupled adsorption and photocatalytic degradation on CAC-TiO_2 composite generating excellent mineralization of alizarin cyanine green dye in aqueous solution," *Arabian Journal of Chemistry*, 2013.

[17] G. Chen and J. Hou, "Photocatalytical elimination of alizarin red by chitosan-Cds composite nanoparticles," *Environmental Science*, vol. 2, no. 1, pp. 56–62, 2007.

[18] J. Zhao, T. Wu, K. Wu, K. Oikawa, H. Hidaka, and N. Serpone, "Photoassisted degradation of dye pollutants. 3. Degradation of the cationic dye rhodamine B in aqueous anionic surfactant/TiO_2 dispersions under visible light irradiation: evidence for the need of substrate adsorption on TiO_2 particles," *Environmental Science & Technology*, vol. 32, no. 16, pp. 2394–2400, 1998.

[19] V. Belessi, G. Romanos, N. Boukos, D. Lambropoulou, and C. Trapalis, "Removal of reactive red 195 from aqueous solutions by adsorption on the surface of TiO_2 nanoparticles," *Journal of Hazardous Materials*, vol. 170, no. 2-3, pp. 836–844, 2009.

[20] E. Kordouli, K. Bourikas, A. Lycourghiotis, and C. Kordulis, "The mechanism of azo-dyes adsorption on the titanium dioxide surface and their photocatalytic degradation over samples with various anatase/rutile ratios," *Catalysis Today*, vol. 252, pp. 128–135, 2015.

[21] Environment Canada and Health Canada, "Screening assessment for the challenge benzenesulfonic acid, 3,3′-[(9,10-dihydro-9,10-dioxo-1,4-anthracenediyl)diimino]bis [2,4,6-trimethyl-, disodium salt] (acid blue 80)," Chemical Abstracts Service Registry 4474-24-2, Environment Canada and Health, 2008, http://www.ec.gc.ca/ese-ees/default.asp?lang=En&n=69053600-1.

[22] N. R. Mathews, E. R. Morales, M. A. Cortés-Jacome, and J. A. Toledo Antonio, "TiO_2 thin films—influence of annealing temperature on structural, optical and photocatalytic properties," *Solar Energy*, vol. 83, no. 9, pp. 1499–1508, 2009.

[23] Y. Pihosh, M. Goto, A. Kasahara, and M. Tosa, "Photocatalytic property of TiO_2 thin films sputtered-deposited on unheated substrates," *Applied Surface Science*, vol. 256, no. 4, pp. 937–942, 2009.

[24] S. H. Hasan, D. Ranjan, and M. Talat, "Water hyacinth biomass (WHB) for the biosorption of hexavalent chromium: optimization of process parameters," *BioResources*, vol. 5, no. 2, pp. 563–575, 2010.

[25] S. Basha and Z. V. P. Murthy, "Kinetic and equilibrium models for biosorption of Cr(VI) on chemically modified seaweed, *Cystoseira indica*," *Process Biochemistry*, vol. 42, no. 11, pp. 1521–1529, 2007.

[26] Y.-S. Ho, "Review of second-order models for adsorption systems," *Journal of Hazardous Materials*, vol. 136, no. 3, pp. 681–689, 2006.

[27] J. Febrianto, A. N. Kosasih, J. Sunarso, Y.-H. Ju, N. Indraswati, and S. Ismadji, "Equilibrium and kinetic studies in adsorption of heavy metals using biosorbent: a summary of recent studies," *Journal of Hazardous Materials*, vol. 162, no. 2-3, pp. 616–645, 2009.

[28] M. A. Hanif, R. Nadeem, H. N. Bhatti, N. R. Ahmad, and T. M. Ansari, "Ni(II) biosorption by *Cassia fistula* (Golden Shower) biomass," *Journal of Hazardous Materials B*, vol. 139, no. 2, pp. 345–355, 2007.

[29] S. Basha, Z. V. P. Murthy, and B. Jha, "Sorption of Hg(II) from aqueous solutions onto *Carica papaya*: application of isotherms," *Industrial & Engineering Chemistry Research*, vol. 47, no. 3, pp. 980–986, 2008.

[30] M. Doğan, H. Abak, and M. Alkan, "Adsorption of methylene blue onto hazelnut shell: kinetics, mechanism and activation parameters," *Journal of Hazardous Materials*, vol. 164, no. 1, pp. 172–181, 2009.

[31] J. B. Condon, Ed., *Measurements and Theory, Elsevier, The Netherlands*, 1st edition, 2006.

[32] C. Villanueva-Jaramillo, A. K. Carrascal-Camacho, M. C. Campos Pinilla, J. C. Salcedo-Reyes, A. E. Florido-Cuellar, and A. M. Pedroza-Rodríguez, "Inactivation of *Escherichia coli* in domestic wastewater using TiO_2/Cu thin films illuminated with white light," in *Proceedings of the 19th International Conference in Photochemical Conversion and Storage of Solar Energy*, Pasadena, Calif, USA, July-August 2012.

[33] A. Hernández, A. K. Carrascal, C. E. Daza, and A. M. Pedroza, "Cu-modified TiO_2-photocatalysis for *Salmonella* spp inactivation," in *Proceedings of the 19th International Conference in Photochemical Conversion and Storage of Solar Energy*, Pasadena, Calif, USA, 2012.

[34] C. Karunakaran, G. Abiramasundari, P. Gomathisankar, G. Manikandan, and V. Anandi, "Cu-doped TiO_2 nanoparticles for photocatalytic disinfection of bacteria under visible light," *Journal of Colloid and Interface Science*, vol. 352, no. 1, pp. 68–74, 2010.

[35] W. Li, R. Liang, A. Hu, Z. Huang, and Y. N. Zhou, "Generation of oxygen vacancies in visible light activated one-dimensional iodine TiO_2 photocatalysts," *RSC Advances*, vol. 4, no. 70, pp. 36959–36966, 2014.

[36] X. Yang, S. Wang, H. Sun, X. Wang, and J. Lian, "Preparation and photocatalytic performance of Cu-doped TiO_2 nanoparticles," *Transactions of Nonferrous Metals Society of China*, vol. 25, no. 2, pp. 504–509, 2015.

[37] D. L. Liao, G. S. Wu, and B. Q. Liao, "Zeta potential of shape-controlled TiO_2 nanoparticles with surfactants," *Colloids and Surfaces A: Physicochemical and Engineering Aspects*, vol. 348, no. 1–3, pp. 270–275, 2009.

[38] I. S. Grover, S. Singh, and B. Pal, "The preparation, surface structure, zeta potential, surface charge density and photocatalytic activity of TiO_2 nanostructures of different shapes," *Applied Surface Science*, vol. 280, pp. 366–372, 2013.

[39] R. K. Gautam, A. Mudhoo, and M. C. Chattopadhyaya, "Kinetic, equilibrium, thermodynamic studies and spectroscopic analysis of alizarin red S removal by mustard husk," *Journal of Environmental Chemical Engineering*, vol. 1, no. 4, pp. 1283–1291, 2013.

[40] A. S. Franca, L. S. Oliveira, V. F. Oliveira, and C. C. O. Alves, "Potential use of *Crambe abyssinica* press cake as an adsorbent: batch and continuous studies," *Environmental Engineering and Management Journal*, vol. 13, pp. 3025–3036, 2014.

[41] S. Dutta, S. A. Parsons, C. Bhattacharjee, P. Jarvis, S. Datta, and S. Bandyopadhyay, "Kinetic study of adsorption and photodecolorization of reactive red 198 on TiO_2 surface," *Chemical Engineering Journal*, vol. 155, no. 3, pp. 674–679, 2009.

[42] N. M. Mahmoodi, B. Hayati, M. Arami, and H. Bahrami, "Preparation, characterization and dye adsorption properties of biocompatible composite (alginate/titania nanoparticle)," *Desalination*, vol. 275, no. 1–3, pp. 93–101, 2011.

[43] K.-J. Hwang, S.-H. Jung, D.-W. Park, S.-J. Yoo, and J.-W. Lee, "Heterogeneous ruthenium dye adsorption on nano-structured TiO_2 films for dye-sensitized solar cells," *Current Applied Physics*, vol. 10, pp. S184–S187, 2010.

[44] I. J. Puentes-Cárdenas, A. M. Pedroza-Rodríguez, M. Navarrete-López, T. L. Villegas-Garrido, and E. Cristiani-Urbina, "Biosorption of trivalent chromium from aqueous solutions by *Pleurotus ostreatus* biomass," *Environmental Engineering and Management Journal*, vol. 11, no. 10, pp. 1741–1752, 2012.

[45] J. Li, J. Feng, and W. Yan, "Excellent adsorption and desorption characteristics of polypyrrole/TiO_2 composite for methylene blue," *Applied Surface Science*, vol. 279, pp. 400–408, 2013.

[46] D. El-Mekkawi and H. R. Galal, "Removal of a synthetic dye 'Direct Fast Blue B2RL' via adsorption and photocatalytic degradation using low cost rutile and Degussa P25 titanium dioxide," *Journal of Hydro-Environment Research*, vol. 7, no. 3, pp. 219–226, 2013.

[47] T.-Y. Kim, J.-W. Lee, E.-M. Jin, J.-Y. Park, J.-H. Kim, and K.-H. Park, "In situ measurement of dye adsorption on TiO_2 thin films for dye-sensitized solar cells," *Measurement*, vol. 46, no. 5, pp. 1692–1697, 2013.

[48] M. L. Yola, T. Eren, N. Atar, and S. Wang, "Adsorptive and photocatalytic removal of reactive dyes by silver nanoparticle-colemanite ore waste," *Chemical Engineering Journal*, vol. 242, pp. 333–340, 2013.

[49] A. Çelekli, G. Ílgün, and H. Bozkurt, "Sorption equilibrium, kinetic, thermodynamic, and desorption studies of reactive red 120 on *Chara contraria*," *Chemical Engineering Journal*, vol. 191, pp. 228–235, 2012.

[50] J. G. Flores-Garnica, L. Morales-Barrera, G. Pineda-Camacho, and E. Cristiani-Urbina, "Biosorption of Ni(II) from aqueous solutions by *Litchi chinensis* seeds," *Bioresource Technology*, vol. 136, pp. 635–643, 2013.

[51] K. Bourikas, M. Stylidi, D. I. Kondarides, and X. E. Verykios, "Adsorption of Acid Orange 7 on the surface of titanium dioxide," *Langmuir*, vol. 21, no. 20, pp. 9222–9230, 2005.

[52] W. Plazinski, W. Rudzinski, and A. Plazinska, "Theoretical models of sorption kinetics including a surface reaction mechanism: a review," *Advances in Colloid and Interface Science*, vol. 152, no. 1-2, pp. 2–13, 2009.

[53] A. Hernández-Estévez and E. Cristiani-Urbina, "Nickel(II) biosorption from aqueous solutions by shrimp head biomass," *Environmental Monitoring and Assessment*, vol. 186, no. 11, pp. 7987–7998, 2014.

[54] C. H. Giles, D. Smith, and A. Huitson, "A general treatment and classification of the solute adsorption isotherm. I. Theoretical," *Journal of Colloid And Interface Science*, vol. 47, no. 3, pp. 755–765, 1974.

[55] G. Limousin, J.-P. Gaudet, L. Charlet, S. Szenknect, V. Barthès, and M. Krimissa, "Sorption isotherms: a review on physical bases, modeling and measurement," *Applied Geochemistry*, vol. 22, no. 2, pp. 249–275, 2007.

[56] H. Yan, H. Li, H. Yang, A. Li, and R. Cheng, "Removal of various cationic dyes from aqueous solutions using a kind of fully biodegradable magnetic composite microsphere," *Chemical Engineering Journal*, vol. 223, pp. 402–411, 2013.

[57] Y. Su, L. Deng, N. Zhang, X. Wang, and X. Zhu, "Photocatalytic degradation of C.I. Acid Blue 80 in aqueous suspensions of titanium dioxide under sunlight," *Reaction Kinetics and Catalysis Letters*, vol. 98, no. 2, pp. 227–240, 2009.

[58] N. Ben-Tal, B. Honig, C. K. Bagdassarian, and A. Ben-Shaul, "Association entropy in adsorption processes," *Biophysical Journal*, vol. 79, no. 3, pp. 1180–1187, 2000.